J Mater Sci: Mater Electron (2025) 36:872

Optimizing the structural, optical, hydrophobic, and electrical properties of (Sn/Mg) co-doped ZnO thin films for application as solar cell electrodes

Imadeddine Bellili[1,*], Warda Darenfad[1], Noubeil Guermat[2,3], and Nadir Bouarissa[4,*]

[1] *Thin Films and Interfaces Laboratory (LCMI), University of Constantine 1, 25000 Constantine, Algeria*
[2] *Department of Electronics, Faculty of Technology, University of M'sila, University Pole, Road Bourdj Bou Arreiridj, 28000 M'sila, Algeria*
[3] *Laboratoire Des Etudes de Matériaux d'Electronique Pour Applications Médicales (LEMEAMED), Université de Constantine 1, 25000 Constantine, Algeria*
[4] *Laboratory of Materials Physics and Its Applications, University of M'sila, 28000 M'sila, Algeria*

Received: 3 January 2025
Accepted: 3 May 2025

© The Author(s), under exclusive licence to Springer Science+Business Media, LLC, part of Springer Nature, 2025

ABSTRACT

A simple chemical pneumatic spray pyrolysis technique was employed to prepare thin films of pure ZnO, 1%Mg-doped ZnO, and co-doped 1%Sn/x%Mg ($x = 1$ and 2) ZnO on ordinary glass substrates at a deposition temperature of 450 °C. The influence of doping and co-doping on the physical properties of the deposited films was systematically investigated. Structural analysis using X-ray diffraction (XRD) and Raman spectroscopy revealed that all samples exhibit a hexagonal crystalline structure with a preferred orientation along the (002) direction, perpendicular to the substrate, with no secondary phases detected. The crystalline quality improved for both doped and co-doped films compared to the undoped ZnO film. Atomic Force Microscopy (AFM) micrographs indicated an increase in surface roughness with doping while co-doping with 1% Sn/1% Mg led to a reduction in roughness compared to pure ZnO. Static contact angle (CA) measurements correlated well with the AFM analysis, showing hydrophobic behavior (CA > 90°) for all elaborated films. This hydrophobic nature is a critical feature for mitigating humidity-induced degradation, thereby enhancing the durability and efficiency of thin-film solar cell layers. Optical analysis demonstrated improved transparency, with average values increasing from 86 to 91%, alongside a widening of the optical bandgap from 3.27 eV to 3.39 eV. The Urbach energy decreased from 329 to 320 meV upon the incorporation of Mg and/or Sn into ZnO. The electrical properties of the ZnO thin films also improved significantly due to the effective incorporation of Sn/Mg, resulting in a low resistivity of 5.44×10^{-3} Ω.cm and a high figure of merit (FOM) of 3.68×10^{-3} Ω^{-1} for the (1%Sn/1%Mg)-ZnO film. Based on the findings of this study, the ZnO:1%Sn:1%Mg film represents the optimal condition for use as a transparent conducting electrode in thin-film solar cells.

Address correspondence to E-mail: imadeddine.billili@doc.umc.edu.dz; n_bouarissa@yahoo.fr

https://doi.org/10.1007/s10854-025-14918-5
Published online: 24 May 2025

1 Introduction

In response to the growing demand for renewable energy, particularly solar cells, the development of efficient storage technologies, such as batteries [1–3] and supercapacitors [4], along with effective conversion solutions based on solar cells, is crucial to ensuring a stable energy supply. Among the metal oxides widely used in photovoltaic cells to enhance light transmission and charge transport are transparent conductive thin films like CdO, SnO_2:F (FTO), In_2O_3:Sn (ITO), and ZnO:Al (AZO). ITO is currently the most commonly used transparent conductive oxide (TCO) in photovoltaic applications, primarily due to its excellent properties, including low resistivity and high transmittance [5, 6]. However, ITO has significant limitations, such as its high toxicity and the limited availability of indium, which is a rare element in nature. These challenges have driven researchers to explore alternative materials. Zinc oxide (ZnO) has garnered considerable attention as a potential replacement for ITO due to its numerous advantages. ZnO is non-toxic, abundant, and features a straightforward deposition process, along with superior durability, making it highly suitable for photovoltaic applications. Furthermore, ZnO exhibits exceptional intrinsic properties, including a wide bandgap of 3.37 eV at room temperature, a high exciton binding energy of 60 meV, and remarkable surface stability [7]. Pure ZnO is frequently utilized as a buffer layer in thin-film solar cells, where it prevents charge recombination by acting as a barrier between the transparent conductive oxide electrode and the absorber layer. However, the intrinsic carriers in undoped ZnO films, predominantly oxygen vacancies (V_O) and zinc interstitials (In_{Zn}) result in low carrier concentrations and high resistivity [8]. These characteristics limit its effectiveness as a transparent conductive layer. To address these limitations, researchers have extensively studied the effects of doping ZnO with various elements. Doping plays a crucial role in optimizing material properties by not only significantly reducing electrical resistivity but also enhancing optical transparency and expanding the optical band gap. These improvements work synergistically to increase the material overall performance as a transparent conducting oxide. For example, Benramache et al. [9] elaborated ZnO thin films doped with 2 wt.% cobalt using the ultrasonic spray technique, achieving a resistivity of 1.20×10^{-1} Ω.cm. Singh et al. [10] employed DC reactive magnetron sputtering to prepare ZnO films doped with 3.2 at.% indium, achieving an exceptionally low resistivity of 3.60×10^{-4} Ω.cm. Additionally, Kuo et al. [11] developed ZnO:x% Al films (x = 0–5) using the sol–gel method. These films exhibited excellent optical transparency ranging from 80 to 95% in the visible wavelength range. Similarly, Guermat et al. [12] reported high transparency levels of up to 93% for ZnO films doped with 3% nickel, which were fabricated using the spray pyrolysis technique. Achieving such a balance requires careful selection of dopants, as well as precise control over their type and concentration, which can significantly influence the physical properties of ZnO and make it a versatile material for optoelectronic applications. Our research is motivated by the challenge of addressing the solubility limitations of individual dopants in the ZnO lattice. Exceeding specific concentration thresholds often leads to undesirable effects such as structural distortions, defect formation, and degradations in the material's physical properties. For instance, magnesium doping should not exceed 3%, cobalt should be limited to 1%, and nickel to 3%. Motivated by this challenge, our research investigates cation-cation co-doping to address the solubility limits of individual dopants. This approach aims to enhance the electrical and optical properties of ZnO while minimizing the risks associated with excessive doping. Through this work, we seek to provide a deeper understanding of the interplay between dopant interactions, solubility, and the resulting physics properties of ZnO thin films. In our recent investigations, we explored the effects of tin (Sn) doping and tin-cobalt (Sn/Co) co-doping on ZnO thin films deposited using the pneumatic spray pyrolysis method [13]. Results revealed that doping with 1%Sn reduced the resistivity to 3.18×10^{-2} Ω.cm while co-doping with 1%Sn/0.5%Co further reduced resistivity to 1.95×10^{-2} Ω.cm, albeit with a minor decrease in transparency from 74 to 71%. These findings underscore the effectiveness of Sn doping in enhancing electrical conductivity, making Sn a promising primary dopant for several reasons. The ionic radius of Sn^{+4} (0.069 nm) is smaller than that of Zn^{+2} (0.074 nm), allowing for efficient substitution within the ZnO crystal lattice. This substitution introduces two additional free electrons by Sn atom, significantly enhancing electrical conductivity [13]. Additionally, tin's abundance and non-toxic nature make it an attractive dopant. Furthermore, Sn doping

improves the thermal and chemical stability of ZnO, further reinforcing its suitability for optoelectronic applications. Building on the success of Sn doping, magnesium (Mg) was introduced as a secondary dopant to further improve transparency and extend the bandgap of ZnO. This extension enhances the absorption of a broader solar spectrum, particularly when ZnO is employed as a carrier transport layer in solar cells. Magnesium was chosen for several reasons: (i) Mg enhances the optical properties of ZnO, ensuring high-quality crystallinity [14]. (ii) The ionic radius of Mg^{+2} (0.066 nm) closely matches that of Zn^{+2}, facilitating its incorporation into the ZnO lattice without significant structural disruption [14]. (iii) Mg is widely available, cost-effective, and non-toxic, aligning with sustainable material development goals. (iv) With an electronegativity value of 1.31, Mg promotes stable crystal structures [15]. For example, Darenfad et al. [14] demonstrated that $Zn_{0.97}Mg_{0.03}O$ film prepared via spray pyrolysis achieved enhanced transmittance of 91% and a bandgap shift to 3.31 eV, making them highly suitable for optoelectronic applications. In this study, the Mg concentration is limited to 2% to avoid exceeding solubility limits, reducing electrical conductivity and causing atomic segregation at grain boundaries. While the individual benefits of Sn and Mg doping are well-documented, there is a lack of comprehensive research on their combined effects in Sn/Mg co-doping. This gap motivated our current study, which seeks to explore the synergistic effects of these dopants on the electrical, optical, and structural properties of ZnO thin films. Among the various physical and chemical methods available for fabricating doped and co-doped ZnO thin films, we employed pneumatic spray pyrolysis due to its simplicity, cost-effectiveness, and capability to produce homogeneous films. This method also facilitates the efficient incorporation of dopants, ensuring the desired modifications in physical properties for diverse applications [14]. Surface wettability is another critical aspect of thin films, especially for optoelectronic applications. Surfaces can be classified as hydrophilic (contact angle < 90°, [16]) or hydrophobic (contact angle > 90°, [17]). Prior studies by Guermat et al. [16], Darenfad et al. [17], and Darenfad et al. [18] demonstrated that hydrophobic, n-type doped oxides, such as SnO_2:12%F, ZnO:6%F:1%Mg, and SnO_2:3%Ni:1%Co, exhibit improved transparency and conductivity. Additionally, hydrophobic surfaces are particularly valuable in reducing humidity-related degradation, enhancing the durability and efficiency of thin-film layers in solar cells. Hydrophobicity ensures optimal sunlight transmission through the transparent layers, improving solar energy conversion efficiency. These compelling results inspired us to explore hydrophobic properties in greater depth.

This study aims to enhance electrical conductivity and achieve excellent transmittance in ZnO thin films co-doped with Sn/Mg. Using a simple and cost-effective pneumatic spray pyrolysis method, we developed hydrophobic ZnO thin films. To our knowledge, this is the first study investigating the wettability of Sn/Mg co-doped ZnO thin films prepared by spray pyrolysis, highlighting the originality of this work. Thus, we seek to explore the effects of Mg doping and Sn/Mg co-doping on ZnO films' structural, topographical, wettability, optical, and electrical properties for use as transparent conductive layers in optoelectronic applications.

2 Experimental Procedure

2.1 Deposition conditions

In our study, thin films were deposited onto ordinary glass substrates using the pneumatic spray technique (Fig. 1). Before the deposition process, the glass substrates underwent a rigorous cleaning procedure to ensure optimal surface preparation and adhesion of the films. The substrates were immersed in acetone, followed by a thorough cleaning with ethanol, and subsequently rinsed with distilled water using ultrasonic cleaning for 15 min, concluding with air drying. The spray solution was produced by dissolving zinc acetate dihydrate [$(CH_3COO)_2Zn{\cdot}2H_2O$] in methanol [$CH_3OH$], obtaining a 0.1 M solution. This solution was continuously stirred at room temperature for one hour. The parameters were consistent for the Mg and Sn/Mg co-doped ZnO thin films. Magnesium acetate [$Mg(CH_3CO_2)_2{\cdot}4H_2O$] and tin chloride [$SnCl_2$] were utilized as the precursors for magnesium and tin dopants, respectively. The weight percent ratio of Sn:Mg dopants relative to Zn was measured at 0:0, 0:1, 1:1, and 1:2. The film deposition was conducted

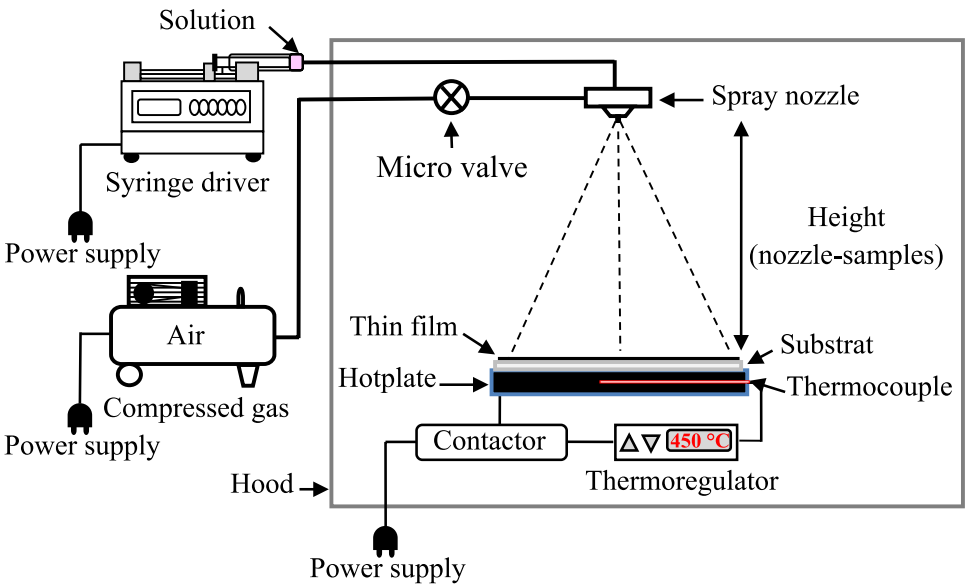

Fig. 1 Schematic diagram of the pneumatic spray technique

under defined parameters: a nozzle-substrate distance of 20 cm and a deposition temperature of 450 °C. Subsequently, the samples will be set up for diverse characterizations.

2.2 Characterization techniques

After the deposition phase, the samples undergo comprehensive analysis to investigate the characteristics of the deposited layers. The crystalline structure of samples was characterized using (PANALYTICAL Empyrean X-ray) diffractometer, employing CuKα radiation ($\lambda = 0.15406$ nm). Raman spectra were acquired via (HORIBA LabRAM HR Evolution) spectrometer at ambient temperature, with a laser source of 473 nm. A DECTAK3 profilometer was employed to measure the films thickness. The topographic characterization was conducted via atomic force microscopy (AFM, MFP-3D Oxford Instruments Asylum Research), with pictures captured in contact mode at ambient temperature in air and examined via AR software. The static contact angle (CA) is measured using a 5 µl droplet at room temperature, with the sample illuminated by a LEYBOLD light source (6 V, 30 W) and recording the CA after 5 s. This measurement assesses the wettability of the thin films. The optical transmittance was measured in the 300 to 800 nm wavelength range by a Shimadzu UV-3101PC UV–Vis-NIR spectrophotometer. The Van der Pauw method was utilized to determine the electrical properties through Hall effect measurements using the Ecopia HMS-3000 device.

3 Results and discussion

3.1 Structural characterizations

3.1.1 X-ray diffraction (XRD) study

To compare the structural properties of different doping concentrations, we conducted X-ray measurements on thin films of 100% ZnO, ZnO:1%Mg, ZnO:1%Mg:1%Sn, and ZnO:2%Mg:1%Sn. The X-ray diffraction spectra of the obtained films are presented in Fig. 2. It is clearly observed that all samples exhibit a sharp and narrow (002) peak, indicating good crystallinity, located at 34.21°. Two additional weak peaks

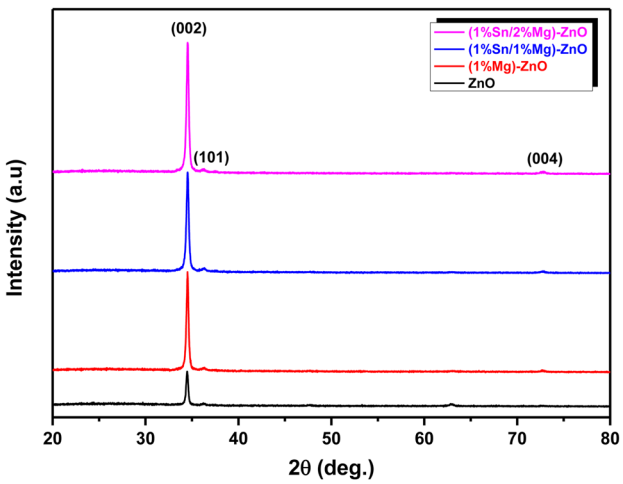

Fig. 2 X-ray diffraction spectra of prepared thin films

at 2θ = 35.85° and 73.54° are also observed, corresponding to the (101) and (004) planes, respectively. According to ASTM files, JCPDS 36–1451 [13], all films are polycrystalline with a hexagonal Wurtzite structure (space group P63mc). No traces of impurities corresponding to MgO, SnO, or SnO_2 are found in the XRD spectra, confirming the purity of the ZnO phase in the prepared films. This behavior aligns well with previous reports in the literature [13, 14]. Furthermore, the hexagonal structure remains unchanged by the doping with Mg and the co-doping with Mg/Sn. To assess the impact of adding Mg and/or Sn dopants to ZnO on the intensity and position of the most intense (002) peak, a zoomed-in view of this peak for 2θ values between 33.7° and 35° is shown in Fig. 3. As Mg and/or Sn are doped into ZnO, the intensity of the (002) peak increases progressively compared to the undoped film, reaching its highest value for the co-doping of 1%Mg:2%Sn. This behavior has also been observed by Darenfad et al. [14] and Zeng et al. [19] for $Zn_{0.97}Mg_{0.03}O$ and ZnO:Mg:Sn films compared to undoped ZnO films prepared by spray pyrolysis and thermal oxidation techniques. The increase in the intensity of the (002) peak is likely due to the enhancement of film crystallinity, suggesting that Sn^{+4} and Mg^{+2} ions are efficiently incorporated into the ZnO matrix and occupy Zn^{+2} sites, leading to a better periodic arrangement of atoms within the lattice. The improved periodicity of the ZnO matrix results in an increase in the diffraction peak intensity. Consequently, the crystallites exhibit a high degree of orientation, with their c-axis perpendicular to the surface. Other researchers have also observed the growth of highly c-axis oriented ZnO films (002) [7, 20]. Additionally, Fig. 3 shows that the position of the peak shifts to higher 2θ values with the addition of Mg and/or Sn dopants compared to 100% ZnO. This shift can be attributed to the decrease in lattice spacing with the increase in Mg concentration. Furthermore, the increase in Mg concentration generates internal strains within the crystal lattice (see Table 1) due to the size difference between Zn^{+2} and Mg^{+2} ions. This size discrepancy creates local distortions in the lattice, affecting the overall crystal geometry. These strains can further reduce the spacing between crystal planes, resulting in an additional decrease in interplanar spacing and, thus, a shift toward higher 2θ values. The same observation was obtained in the study by Darenfad et al. [14], who developed pure ZnO, $Zn_{0.97}Mg_{0.03}O$ and $Zn_{0.96}Mg_{0.03}Mn_{0.01}O$ films. The d-spacing equation for the hexagonal crystal structure was used to calculate the lattice parameter c. This equation can be simplified to $c = \frac{\lambda}{\sin\theta(002)}$. The stress (σ) has been calculated using the equation [13]:

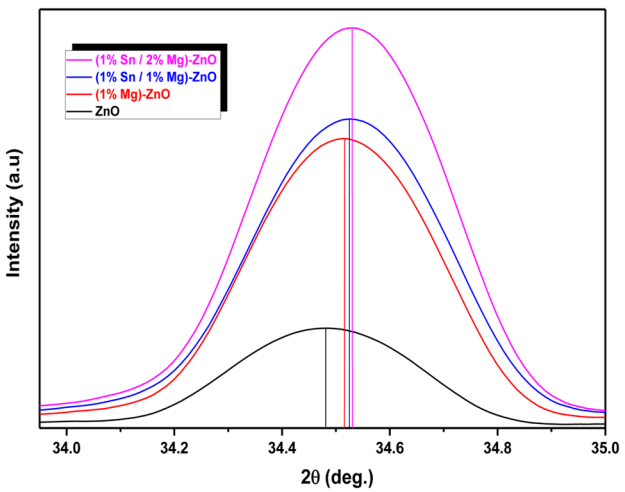

Fig. 3 Enlargement of the XRD spectra near the (002) peak for the films analyzed

$$\sigma = \frac{-233(c - c_0)}{c_0} \quad (1)$$

where $c_0 = 0.52066$ nm, and σ is in GPa, c and σ values are provided in Table 1. All the films exhibit a

Table 1 Structural parameters of obtained films

Samples	(002) peak position, 2θ (°)	Lattice parameter, c (nm)	FWHM, β (°)	Crystallite size, D (nm)	Stress, σ (GPa)	Dislocation density, δ ($\times 10^{-3}$ nm^{-2})
ZnO	34.45	0.5202	0.2269	38	0.1987	0.68
1%Mg-ZnO	34.49	0.5197	0.2420	36	0.4144	0.78
1%Sn/1%Mg-ZnO	34.50	0.5196	0.2652	33	0.4797	0.92
1%Sn/2%Mg-ZnO	34.50	0.5195	0.2598	33	0.5093	0.90

reduction in the c-axis lattice parameter, as shown in Table 1. This reduction indicates the presence of structural stresses across all the films. Compared to pure ZnO, the observed decrease in the c-parameter and the corresponding increase in stress values can be attributed to two primary factors.

The primary explanation is that the ionic radii of Sn^{+4} (0.069 nm) and Mg^{+2} (0.066 nm) are less than those of Zn^{+2} (0.074 nm) [20, 21]. The second probable reason is the considerable difference in electronegativity between the Zn^{+2} (1.65) and Mg^{+2} (1.31) ions, resulting in a significant attraction among the Mg^{+2} and O^{-2} ions, which may have reduced the c-axis. Comparable behavior was likewise noted by El Hamidi et al. [22] and Aslan et al. [23]. Both instances provide compelling evidence for the suitable integration of Sn^{+4}/Mg^{+2} ions into the ZnO lattice. Furthermore, the observed increase in strain can be explained by the combined effects of doping and co-doping, which promote the appearance of intrinsic defects in the material. One of the main mechanisms is the creation of oxygen vacancies resulting from the substitution of Zn^{+2} ions by Mg^{+2} ions. These vacancies arise due to the smaller ionic radius of Mg^{+2} ions, which causes a local disruption of the crystal lattice. Furthermore, the addition of Sn^{+4} ions causes significant deformation in the crystal lattice due to their higher charge compared to Zn^{+2} ions. The average crystallite size (D) and dislocation density (δ) of the films were determined using the equations [24, 25]:

$$D = \frac{0.9\lambda}{\beta \cos\theta} \tag{2}$$

$$\delta = \frac{1}{D^2} \tag{3}$$

where λ stands for the X-ray's wavelength, β pertains to the full width at half maximum (FWHM) of the diffraction peak, θ indicates the diffraction angle. Regarding the values presented in Table 1, the crystallite sizes of Mg-doped and Sn/Mg co-doped ZnO films are smaller compared to undoped ZnO. This reduction in crystallite size is attributed to the incorporation of dopants into the ZnO crystal lattice, which disrupts the natural growth process by increasing the density of nucleation sites, ultimately resulting in smaller crystallites. These findings are consistent with existing literature [12, 18]. Furthermore, this decrease in crystallite size can be explained by an increase in dislocation density (see Table 1), as higher nucleation rates during the early stages of film growth tend to generate more defects in the crystal structure, contributing to smaller crystallites.

3.1.2 *Raman spectroscopy study*

Raman spectroscopy is a powerful, non-destructive characterization technique that provides information concerning the structural characteristics, electronic properties, and level of disorder in a crystal resulting from dopant inclusion. The structural irregularity is evident in the line shape, including line intensity, width, and frequency.

Figure 4 illustrates the Raman spectra of the synthesized thin films within the wavenumber range of 80–700 cm^{-1}. For the undoped ZnO thin-film, characteristic vibrational modes are observed at 98 cm^{-1}, 435 cm^{-1}, and 554 cm^{-1}, corresponding to the E_2(low), E_2(high), and A_1(LO) modes, respectively. These dominant Raman modes serve as key indicators of the hexagonal wurtzite crystal structure of ZnO, confirming its structural integrity [26]. The Raman spectra of the co-doped ZnO films reveal additional peaks at 223 cm^{-1} and 274 cm^{-1}, attributed to the $2E_2$(low) and B_1 vibrational modes, respectively. These supplementary peaks are associated with the presence of Sn impurities incorporated into the ZnO crystalline lattice, as reported in similar studies [13, 27]. Relative to pure ZnO spectra, E_2(low) and E_2(high) intensities diminish with doping and co-doping. This is attributed to the alteration in lattice compression along the c-axis

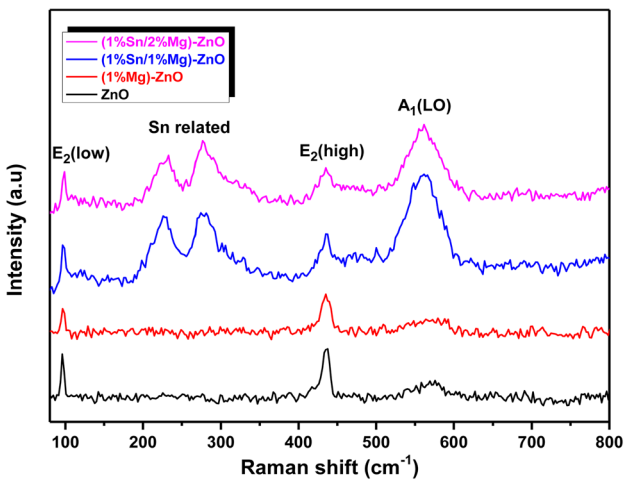

Fig. 4 Raman spectra of obtained thin films

due to the substitution of Sn^{+4} and Mg^{+2} ions, which possess smaller ionic radii (0.069 nm and 0.066 nm, respectively) in place of Zn^{+2} (0.074 nm) in the ZnO matrix. Furthermore, the significant disparity in electronegativity between Zn^{+2} (1.65) and Mg^{+2} (1.31) ions reduces the Zn–O bond. A rise in A_1(LO) intensity is evident with Mg-doping. An even more pronounced increase occurs with (1%Sn/1%Mg) co-doping (Fig. 4). The amplification of the A_1(LO) mode, prompted by oxygen vacancies or Zn interstitials caused by doping and co-doping, thereby increasing the carrier density that interacts with the macroscopic electric field generated by (LO) phonons, known as Frohlich interaction [28, 29]. The elevation of Mg concentration in (1%Sn/2%Mg)-ZnO film resulted in a decrease in A_1(LO) intensity. This decrease can be attributed to the compensatory effects arising from increased Mg content, which constrains the effectiveness of co-doping. The rectification of defects may lead to a decrease in the total defect density within the material. Consequently, the electron–phonon coupling associated with the A_1(LO) mode may be less affected, resulting in a reduction in their intensity [30].

3.2 Surface topography

The surface topography of our thin films was examined by AFM micrographs taken on the 20 µm × 20 µm area. The two-dimensional (2D) and three-dimensional (3D) AFM images of undoped ZnO, 1%Mg-doped, and (1%Sn/1%Mg) co-doped ZnO films are illustrated in Fig. 5. It is evident that the undoped ZnO film (Fig. 5(a)) has a low density, uniformly and inhomogeneous grains distributed over the surface of the substrate. The surface morphology is strongly affected by Mg doping and Sn/Mg co-doping, as shown in the 2D image Fig. 5(b); the surface of the 1%Mg-ZnO sample had a homogeneous granular nature with agglomerated grains while the (1%Sn/1%Mg)-ZnO film Fig. 5(c) have a smaller grains size, a more homogeneous and compact densely packed surface. According to the 3D micrographs, the (1%Mg) doped and (1%Sn/1%Mg) co-doped ZnO films exhibit columnar growth characteristics in the form of cones, with uniformly distributed grains on the surface of the samples (Figs. 5(b) and (c)).also, the (1%Sn/1%Mg)-ZnO film has a relatively smoother surface, with a decrease in the grains roughness. The columnar structure of the films is due to the crystallites growth along c-axis direction perpendicular to the surface. This agrees with the XRD results indicating the crystallite's preferential orientation along the (002) plane.

The mean square roughness (RMS) is one of the important parameters of ZnO thin films since a smooth surface can reduce the scattering of incident light, improving the surface's optical quality [31] and also contributes to reducing its resistivity. As evident from Fig. 5, the RMS of the undoped and (1%Mg)-ZnO films are found to be 4.75 and 10.13 nm, respectively. The increase in surface roughness is likely the consequence of an agglomeration of grains. The minor roughness is obtained for sample (1%Sn/1%Mg)-ZnO with a value (RMS = 3.53 nm) due to its smallest crystallite size (D = 33 nm), exhibiting the highest quality surface morphology for TCO use.

3.3 Wettability study

Figure 6 illustrates static contact angle (CA) images for various films elaborated using pneumatic spray deposition. Specifically, Fig. 6(a) shows a contact angle of 91° for the undoped ZnO, Fig. 6(b) reveals a CA of 125° for the ZnO:1%Mg, Fig. 6(c) presents a CA of 107° for ZnO:1%Sn:1%Mg, and Fig. 6(d) displays a CA of 112° for ZnO:1%Sn:2%Mg. These results indicate a hydrophobic nature (CA > 90°) for all the films studied. A similar trend in hydrophobic behavior was observed and reported by Darenfad et al. [17] during their study of thin films of pure ZnO, ZnO:1%Mg, and ZnO:6%F:1%Mg deposited by spray pyrolysis. According to Darenfad et al. [17], this hydrophobic character arises from the surface morphology of the films when interacting with water droplets. These results can be further understood through the Cassie-Baxter model [32], which posits that air pockets trapped between the water droplet and the textured surface contribute to an increased contact angle. In this study, Mg-doping introduced surface roughness to the ZnO films, promoting greater air entrapment and thereby enhancing their hydrophobic properties. Furthermore, co-doping with Sn and Mg also led to preferred crystallographic orientations, resulting in surface structures with conical elongations. These elongated features elevate water droplets, causing them to rest on the peaks of the surface ridges and minimizing adhesion. The enhanced surface morphology resulting from Mg and/or Sn doping not only improved hydrophobicity but also provided functional advantages in practical applications, particularly in the development of transparent electrodes for solar cells [17].

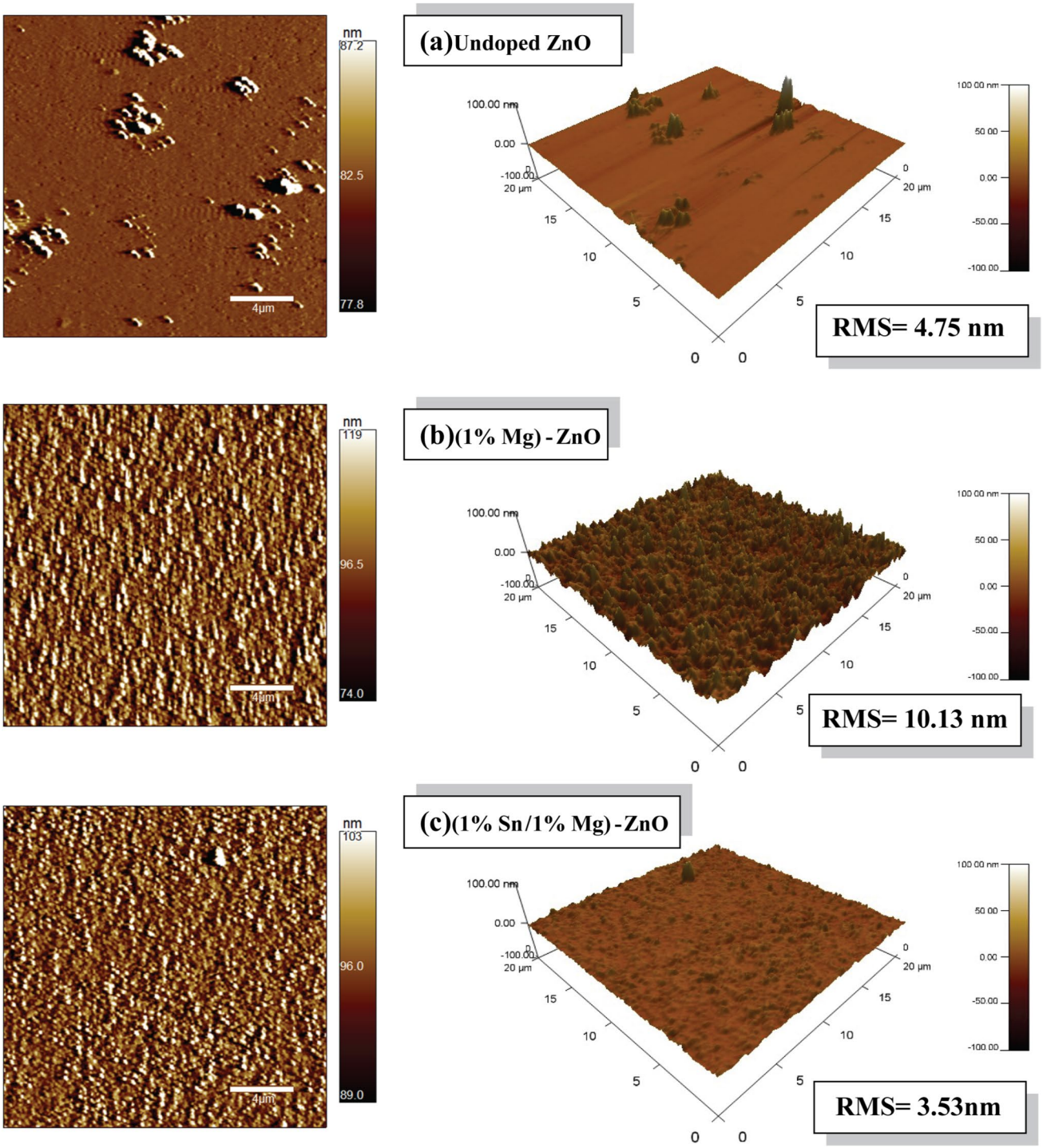

Fig. 5 Surface topography images of prepared thin films

Hydrophobic surfaces not only facilitate the deposition and adhesion of subsequent layers but also enhance the overall fabrication process by ensuring uniform coatings. Furthermore, such surfaces exhibit superior chemical and electrical stability, which reduces the risk of degradation due to exposure to moisture or environmental contaminants. These findings align with the AFM analysis shown in Fig. 5,

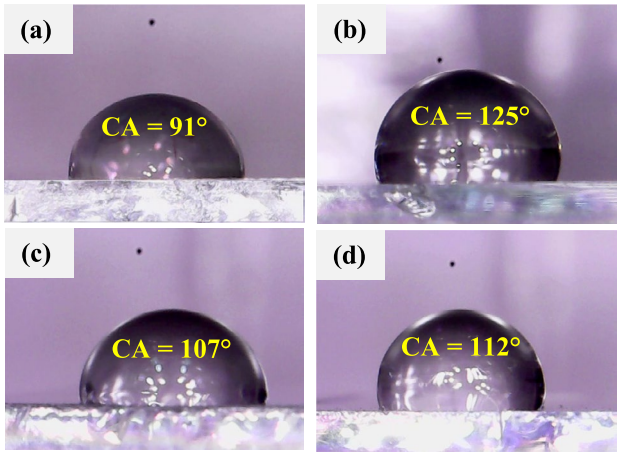

Fig. 6 Contact angles of **a** undoped ZnO, **b** ZnO:1%Mg, **c** ZnO:1%Sn:1%Mg, and **d** ZnO:1%Sn:2%Mg elaborated thin films

further confirming the correlation between surface morphology and the hydrophobic properties of the films.

3.4 Optical study

Optical transmittance is a crucial parameter in transparent conducting oxides. Figure 7 displays the transmittance spectra recorded in the wavelength range from 330 to 800 nm of our spray-deposited layers. All samples exhibit high transparency in the visible spectrum, indicating the films' smooth surfaces [14]. This further corroborates the prior AFM microscopy findings. The plots illustrate interference fringes at different wavelengths. The persistent oscillation of maxima and minima at varying wavelengths, attributable to layer thickness (Table 2), confirms the optical homogeneity of the deposited thin films. Furthermore, the transmittance is enhanced with doping and co-doping relative to that of pure ZnO. The average transmission value for undoped ZnO was roughly 86%, whereas the (1%Sn/2%Mg) co-doped ZnO film achieved an average of 91% (Table 2). The increase may occur from the successful incorporation of Mg and Sn within the ZnO structure, which improves the crystallinity of films, as revealed by X-ray diffraction data. Furthermore, this behavior can be attributed to the hydrophobic nature of the doped and co-doped films, as illustrated in Fig. 6. The inherent hydrophobicity of these films promotes better interaction with their environment, leading to a positive impact on their optical properties. This phenomenon is consistent with observations reported in other studies, particularly those focusing on the optoelectronic characteristics of ZnO thin films doped with magnesium or co-doped with magnesium and fluorine elaborated by spray pyrolysis [17]. It is also noticed that all the films display a sharp absorption edge, corresponding to fundamental absorption attributed to inter-band electronic transitions, observed around 375–379 nm, indicating significant UV light absorption, which suggests the potential application of (Sn/Mg) co-doped ZnO in UV detection. The sharp absorption edge, indicative of a direct bandgap material, demonstrates blue shifts with doping and co-doping, signifying an expansion in the bandgap energy. The films optical band gap (E_g) may be determined utilizing the Tauc relation [33]:

$$(\alpha h\nu)^2 = A(h\nu - E_g) \quad (4)$$

Where α is the absorption coefficient, hν is the photon energy, and A is a constant. The band gap

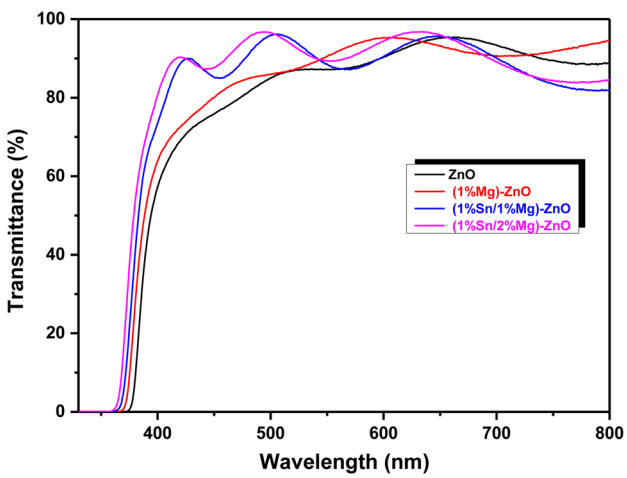

Fig. 7 Optical transmittance spectra of obtained films

Table 2 Thickness, transmittance, optical gap, and Urbach energy values of prepared films

Samples	Thickness, d (nm)	Transmittance, T (%)	Optical gap, Eg (eV)	Urbach energy, E_U (meV)
ZnO	544	86	3.27	329
1%Mg-ZnO	548	88	3.31	327
1%Sn/1% Mg-ZnO	638	89	3.35	325
1%Sn/2%Mg-ZnO	657	91	3.39	320

represents the intersection between the linear part of the Tauc plots and the photon energy axis, as shown in Fig. 8. The band gap values (Table 3) ranged from 3.27 to 3.39 eV, influenced by variations in dopants concentrations. The expansion in the ZnO band gap through the incorporation of Mg and Sn can be ascribed to various mechanisms: Initially, metal precursors were added at Zn sites. Due to the difference in electronegativity between Zn/Mg and the ionic radius between Mg/Sn and Zn induces a reduction in the lattice parameter, hence widening the optical band gap [22]. This increase can be explained by the inherently high optical bandgaps of MgO and SnO_2, which are 7.7 eV and 4 eV, respectively. These values significantly influence the bandgap of ZnO when Mg^{+2} and Sn^{+4} ions are incorporated into its crystalline structure. The increase in E_g is attributed to the reduction in D (Table 1), which can be explained by the effects of quantum confinement, crystal lattice strain, the reduction of defect states, and the Moss-Burstein effect [34]. Introducing Sn^{+4} and Mg^{+2} ions into the ZnO crystal lattice creates supplementary energy levels and electrons, altering the fermi level and resulting in a blue shift due to enhanced radiative recombination of excitons. This band gap expansion has been referenced in numerous other researches [34, 35].

The Urbach tail energy (E_U) is an important measure for characterizing a material's disorder. The E_U values were obtained from the slant of the ln (αhv) graph vs photon energy (Fig. 9) by applying the formula [14].

Table 3 Carrier concentration, Hall mobility, and resistivity of elaborated samples

Samples	Carrier concentration, $\times 10^{18}$ (cm^{-3})	Mobility, (cm^2 V^{-1} s^{-1})	Resistivity, $\times 10^{-2}$ (Ω.cm)
ZnO	3.97	11.01	14.27
1% Mg-ZnO	20.84	1.17	18.78
1%Sn/1%Mg-ZnO	745.80	1.54	0.54
1%Sn/2%Mg-ZnO	53.54	3.74	3.12

$$\alpha = \alpha_0 \exp\left(\frac{h\nu}{E_u}\right) \quad (5)$$

Where α_0 denotes a constant, h represents Planck's constant, E_U pertains to Urbach energy, and υ indicates the frequency. The Urbach energy values for prepared films are regrouped in Table 2. According to Table 2, the Urbach energy ranges between 320 and 329 meV, depending on the specific doping and co-doping levels, and demonstrates a significant reduction compared to the undoped ZnO film. This reduction is closely linked to the improvement in the crystalline quality of the material, as evidenced in Fig. 2. Moreover, this decrease in E_U is primarily attributed to the widening of the optical band gap, which plays a pivotal role in reducing the density of localized electronic states within E_g. A broader optical band gap reflects an enhanced structural organization and reduced structural disorder in the material,

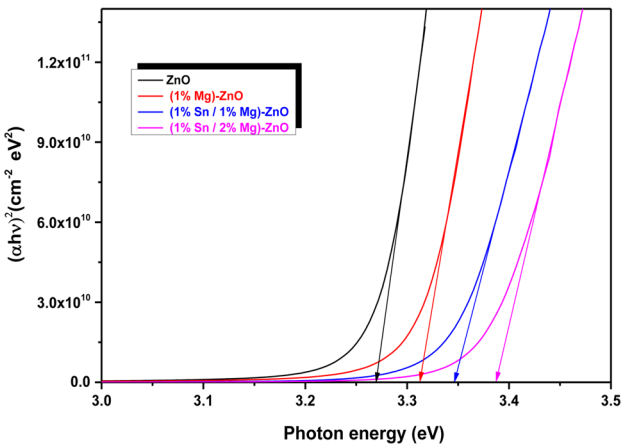

Fig. 8 Plot of $(\alpha h\upsilon)^2$ against (hυ) for obtained films

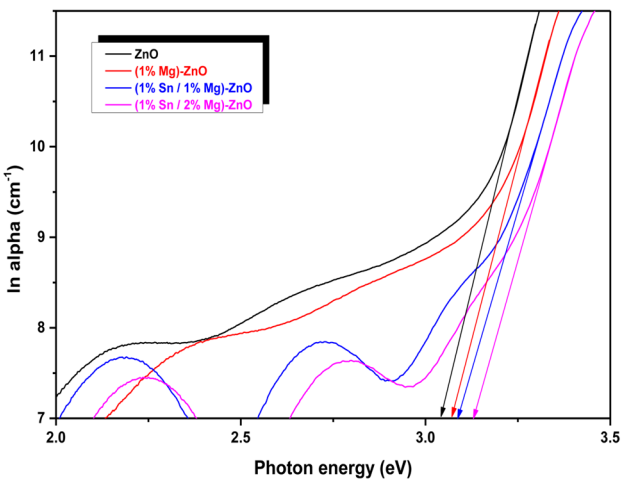

Fig. 9 Variation of ln(α) with photon energy (hυ) for obtained films

indicating a more ordered and coherent crystal network. Moreover, the observed reduction in localized states correlates with a significant decrease in surface roughness, as illustrated in Fig. 5. A smoother surface promotes better uniformity and homogeneity at the nanoscale level, which enhances both the optical and electronic properties of the material. As the structure becomes more ordered, several benefits arise, including improved transparency and enhanced charge conduction. These improvements are particularly advantageous for applications where the material functions as a transparent electrode in solar cells.

3.5 Electrical properties

The influence of Mg and (Sn/Mg) content on carrier concentration (n), Hall mobility (μ), and electrical resistivity (ϱ) of our samples were analyzed utilizing Hall effect measurements by van der Pauw's method. The electrical characteristics were measured at room temperature and are summarised in Table 3. All the films exhibit n-type conductivity. From Table 3, it is evident that the electrical resistivity of ZnO films is significantly influenced by both the type and concentration of the dopants introduced. Specifically, the addition of Mg to the ZnO matrix led to an increase in the resistivity of the thin films. This observation is consistent with previous reports in the literature [14, 36]. The increase in the resistivity of the thin films by Mg-doping can be explained by the reduction in carrier mobility. This reduction is strongly influenced by the surface morphology of the thin-film, ultimately leading to an increase in the resistivity of the ZnO:Mg film. AFM analyses further support this observation, revealing that the ZnO/Mg film exhibits the highest roughness value among the samples studied, with an RMS of 10.13 nm. The resistivity of the thin ZnO:Mg film ($\rho = 1.878 \times 10^{-1}$ Ω.cm) obtained in this study using the pneumatic spray was found to be significantly lower compared to similar films doped with Mg and elaborated by the sol–gel, which exhibit a resistivity on the order of $2.5 \times 10^{+6}$ Ω.cm [36]. According to the same figure, the addition of Mg at concentrations of x% ($x = 1$ and 2) to ZnO:1%Sn significantly improves the electrical conductivity and increases the charge carrier concentration compared to 100% ZnO films and Mg-doped ZnO films. Among these, the ZnO:1%Sn:1%Mg film exhibits the lowest electrical resistivity of 5.44×10^{-3} Ω.cm and the highest charge carrier concentration, measured at $7.458 \times 10^{+20}$ cm^{-3}. A similar trend of improved electrical conductivity in co-doped ZnO films has been observed by Lee et al. [37] in Sn/Al co-doped ZnO thin films, by Tiwari and Sahay [38] in Sn/Ga co-doped ZnO films, by Tiwari et al. [39] in Sn/Ni co-doped ZnO thin films, by Ma et al. [40] in Na/Mg co-doped ZnO thin films, and by Guermat et al. [12] in Co/Ni co-doped ZnO thin films. This enhancement in conductivity can be attributed to two main factors: (i) The cations (Sn^{+4}, Mg^{+2}) act as donors and are incorporated into the substitutional or interstitial sites of Zn^{+2}, which increases the free electron concentration and facilitates electrical conduction. For instance, the substitution of each Sn^{+4} ion on the Zn^{+2} site generates two additional free carriers. On the other hand, the incorporation of Mg^{+2} ions into the ZnO lattice results in an increase in electron density due to the lower electron affinity of MgO compared to ZnO. (ii) The second factor is the co-doping process (1%Sn/1%Mg-ZnO), which induces the formation of intrinsic defects such as oxygen vacancies (V_o) and interstitial zinc atoms (Zn_i). Oxygen vacancies act as donor sites, increasing the density of free carriers (Table 3). This enhanced carrier density effectively reduces the resistivity of the ZnO thin-film. The interaction between these defects and the dopant ions is consistent with Raman spectroscopy results and optical studies, confirming their essential role in improving conductivity. Furthermore, the denser and more homogeneous surface of the (1%Sn/1%Mg)-ZnO thin-film is beneficial in reducing resistivity [18], which is in good agreement with the AFM analysis (Fig. 5). However, when the Mg concentration was increased to 2% in the ZnO:1%Sn film, a gradual decrease in carrier concentration was observed, leading to a corresponding increase in resistivity (see Table 3). Similar trends have been reported in ZnO co-doped films by Darenfad et al. [14], Zhang et al. [41], and Yılmaz et al. [42]. The increase in resistivity observed in the ZnO:1%Sn:2%Mg film is primarily due to the inherently resistive nature of MgO, which becomes more pronounced when the Mg concentration exceeds an optimal threshold. Additionally, the increase in resistivity is also attributed to a reduction in donor defects, such as oxygen vacancies, which are essential for maintaining high carrier concentrations. A detailed comparison of the optical and electrical properties of the ZnO:1%Mg:1%Sn thin-film with those reported in the literature, produced using various deposition methods, is presented in Table 4. This table highlights the significant improvement in the electrical performance of the ZnO:1%Mg:1%Sn film obtained by incorporating 1%Mg as a dopant into the ZnO:1%Sn lattice.

Table 4 A comparison of transmittance and electrical properties of (Mg/Sn) co-doped ZnO thin-film with previous reports

TCO Material	Technique of fabrication	Transmittance, (%)	Resistivity, (Ω.cm)	Ref
$Zn_{0.97}Mg_{0.03}O$	Spray pyrolysis	91.06	$1.8\times10^{+2}$	[14]
$Zn_{0.96}Mg_{0.04}O$	Sol–gel	85	$2.5\times10^{+6}$	[36]
ZnO:1%Sn	Pneumatic spray	77	3.18×10^{-2}	[13]
ZnO:1%Sn:0.5%Co	Pneumatic spray	73	1.95×10^{-2}	[13]
$Zn_{0.91}Mg_{0.03}F_{0.06}O$	Spray pyrolysis	80	$1.11\times10^{+2}$	[17]
$Zn_{0.96}Mg_{0.03}$ $Mn_{0.01}O$	Spray pyrolysis	84.01	3.24×10^{-1}	[14]
ZnO: 5at Mg:2 at%Ga	RF magnetron sputterin	85	5.76×10^{-3}	[43]
ZnO:1at%Sn:1at%Mg	Sol–gel	~95	7.24×10^{-3}	[44]
ZnO:1%Sn:1%Mg	Pneumatic spray pyrolysis	89.05	5.44×10^{-3}	Present work

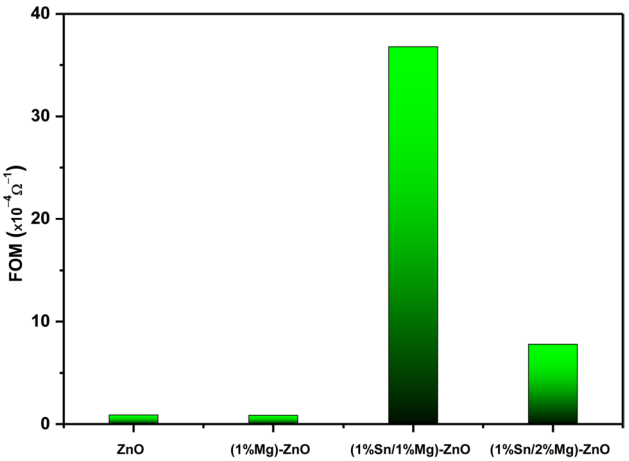

Fig. 10 Alteration of the FOM for obtained thin films

In order to evaluate the performance of films doped with Mg and co-doped with (Sn/Mg) for optoelectronic applications, it is essential to determine the figure of merit (FOM) utilizing Haacke's formula [13]:

$$FOM = \frac{T^{10}}{R_s} \tag{6}$$

Where T represents the average transmittance within the wavelength range of 400 to 800 nm, while R_s denotes the sheet resistance of the film, these parameters are crucial for evaluating the optoelectronic performance of thin films. Figure 10 provides a comparative overview of the FOM values for our films. A higher FOM value indicates superior film quality, reflecting an optimal balance between high optical transparency and low electrical resistance. The FOM initially diminished with Mg doping, ascribed to its high electrical resistivity relative to undoped ZnO. All (Sn/Mg) co-doped films exhibited elevated figures of merit, indicating enhanced optoelectronic features, particularly the (1%Sn/1%Mg)-ZnO film, which demonstrates an optimal FOM value of $3.68 \times 10^{-3}\ \Omega^{-1}$, signifying its superior optoelectronic performance. Interestingly, this FOM value is more significant than other films synthesized using other deposition techniques, as demonstrated in Table 5.

4 Conclusions

In summary, we successfully synthesized nanocrystalline thin films of pure ZnO, ZnO:1%Mg, ZnO:1%Sn:1%Mg, and ZnO:1%Sn:2%Mg using a simple pneumatic spray pyrolysis technique. The effects of Mg and/or Sn doping on the physical properties of the films were thoroughly investigated. X-ray diffraction (XRD) analysis confirmed the

Table 5 A comparative analysis of the FOM of (1% Sn/1% Mg) co-doped ZnO thin-film with earlier researches

TCO thin-film	Deposition Technique	FOM, (Ω^{-1})	Ref
ZnO:3 at.% Sn	Spin-coating	8×10^{-9}	[45]
ZnO:6 at.% Sn	Spin-coating	8.5×10^{-4}	[46]
1.16 at.% Ga-ZnO	Atomic layer deposition	$3.5\ 10^{-3}$	[47]
(1%Sn/0.5%Co)-ZnO	Spray pyrolysis	1.41×10^{-4}	[13]
ZnO:1wt.% Al/1wt.% Sn	Spray pyrolysis	$1.69\ 10^{-4}$	[27]
ZnO:1%Sn:1%Mg	Pneumatic spray pyrolysis	3.68×10^{-3}	This work

hexagonal wurtzite structure of ZnO, characterized by a dominant (002) diffraction peak. The increased intensity of this peak with the incorporation of Mg and/or Sn indicates an enhancement in the crystalline quality of the films. Additionally, the absence of secondary phases confirms the high purity of the synthesized samples. Raman spectroscopy further validated the formation of the wurtzite structure across all deposited films. Atomic force microscopy (AFM) analysis revealed the influence of the dopants on surface morphology. Among the synthesized films, ZnO:1%Sn:1%Mg exhibited the lowest surface roughness, indicating a smoother surface compared to other films. Static contact angle (CA) measurements demonstrated values exceeding 90°, highlighting the hydrophobic nature of the films, an essential property for thin-film solar cell applications. Optical transmittance measurements showed a significant increase in transparency with the introduction of Mg and/or Sn dopants compared to pure ZnO. Notably, the hydrophobic nature (CA > 100°) of ZnO:1%Sn:1%Mg and ZnO:1%Sn:2%Mg films enhanced their optical transmission to 89% and 91%, respectively, compared to 88% for Mg-doped films in the wavelength range of 400–800 nm. Doping and co-doping also resulted in a notable widening of the ZnO bandgap, from 3.27 eV to 3.39 eV, along with a reduction in Urbach energy from 329 to 320 meV relative to pure ZnO films. Electrical measurements of the co-doped films revealed significant improvements in conductivity. The ZnO:1%Sn:1%Mg film exhibited a low resistivity of 5.44×10^{-3} Ω.cm, a high carrier concentration of $7.458 \times 10^{+20}$ cm^{-3}, and an impressive figure of merit of 3.68×10^{-3} Ω^{-1}. In conclusion, the incorporation of Mg and/or Sn as dopants in ZnO films improves the crystal structure of the films, improves their hydrophobicity, contributes to a smoother surface morphology, and elevates their optical and electrical performance. Among the different samples studied, the nanocrystalline film of ZnO co-doped with 1% Sn and 1% Mg appears particularly remarkable. It presents exceptional transparency, a widened optical band gap, a low resistivity, a high concentration of carriers charge and a high figure of merit. These exceptional optoelectronic characteristics position this material as an ideal candidate for advanced applications in thin-film solar cells, particularly as a transparent conductive electrode.

Author contributions

All authors contributed to the study conception and design. Material preparation, data collection and analysis were performed by IB, WD, NG and NB. The first draft of the manuscript was written by WD, and all authors commented on previous versions of the manuscript. All authors read and approved the final manuscript.

Data availability

The data that support the findings of this study are available from the corresponding author on reasonable request or as per journal policy.

Declarations

Competing interests The authors declare that they have no known competing financial interests or personal relationships that could have appeared to influence the work reported in this paper.

Ethical approval The authors declare that they have no known competing financial interests or personal relationships that could have appeared to influence the work reported in this paper. The manuscript has not been published previously and is not under consideration for publication. It is also stated that the work is original. The publication is approved by all authors and tacitly or explicitly by the responsible authorities where the work was carried out. If accepted, it will not be published elsewhere in the same form, in English or in any other language, including electronically without the written consent of the copyright holder. In addition, the authors have no conflicts of interest nor data fabrication or reproducibility concerns and plagiarism.

References

1. M.Z. Arif, N. Iqbal, R. Mahek, T. Noor, A. Khan, Molybdenum-doped lithium vanadium phosphate ($Li_3Mo_xV_{2-x}(PO_4)_3$/C) as cathode material in lithium ion batteries. J. Mater. Sci. Mater. Electron. **32**, 16669–16681 (2021). https://doi.org/10.1007/s10854-021-06222-9

2. P.P. Badami, M.Z. Arif, D. Rettenwander, C.K. Chan, A.M. Kannan, Synthesis of Li7La3Zr2O12 Li-Ion conducting electrolytes by a Rapid solution-combustion method, A05: advances, challenges, and development of solid state battery electrochemistry and materials. ECS Meet Abstr (2020). https://doi.org/10.1149/MA2020-025941mtgabs
3. M.Z. Arif, A.E. Imel, B. Barth, T.A. Zawodzinski, Probing the process of electron transfer in microemulsions with substituted ferrocenes. ECS Meet Abstr (2024). https://doi.org/10.1149/MA2024-021142mtgabs
4. A. Imel, Z.Z. Arif, B. Barth, G. Goenaga, T.A. Zawodzinski, 2024 Enhancing Supercapacitor Performance with Microemulsion-Based Electrolytes. MA2024–02 (2024) 680. https://doi.org/10.1149/MA2024-026680mtgabs
5. S. Marikkannu, M. Kashif, N. Sethupathy, V.S. Vidhya, S. Piraman, A. Ayeshamariam, M. Bououdina, N.M. Ahmed, M. Jayachandran, Effect of substrate temperature on indium tin oxide (ITO) thin films deposited by jet nebulizer spray pyrolysis and solar cell application. Mater. Sci. Semicond. Process. **27**, 562–568 (2014). https://doi.org/10.1016/j.mssp.2014.07.036
6. M. Thirumoorthi, Structure, optical and electrical properties of indium tin oxide ultra thin films prepared by jet nebulizer spray pyrolysis technique. J. Asian Ceram. Soc. **4**, 124–132 (2016). https://doi.org/10.1016/j.jascer.2016.01.001
7. J.H. Gu, H. Long, S.B. Chen, Z.Y. Zhong, Microstructural characterization and physical properties of transparent conducting magnesium–titanium co-doped zinc oxide thin films. J. Mater. Sci. Mater. Electron. **33**, 25219–25231 (2022). https://doi.org/10.1007/s10854-022-09226-1
8. Z. Li, J. Li, M. Xiong, J. Lei, Y. Chen, S. Zhang, Effects of Mo single-doping and Mo-Al co-doping on ZnO transparent conductive films. Appl. Surf. Sci. **584**, 152588 (2022). https://doi.org/10.1016/j.apsusc.2022.152588
9. S. Benramache, B. Benhaoua, O. Belahssen, The crystalline structure, conductivity and optical properties of Co-doped ZnO thin films. Optik **125**, 5864–5868 (2014). https://doi.org/10.1016/j.ijleo.2014.07.055
10. A. Singh, S. Chaudhary, D.K. Pandya, High conductivity indium doped ZnO films by metal target reactive co-sputtering. Acta Mater. **111**, 1–9 (2016). https://doi.org/10.1016/j.actamat.2016.03.012
11. S.Y. Kuo, W.C. Chen, F.I. Lai, C.P. Cheng, H.C. Kuo, S.C. Wang, W.F. Hsieh, Effects of doping concentration and annealing temperature on properties of highly-oriented Al-doped ZnO films. J. Cryst. Growth **287**, 78–84 (2006). https://doi.org/10.1016/j.jcrysgro.2005.10.047
12. N. Guermat, W. Daranfed, I. Bouchama, N. Bouarissa, Investigation of structural, morphological, optical and electrical properties of Co/Ni co-doped ZnO thin films. J. Mol. Struct. **1225**, 129134 (2021). https://doi.org/10.1016/j.molstruc.2020.129134
13. I. Bellili, M. Mahtali, W. Darenfad, N. Guermat, The figure of merit improvement of (Sn, Co)-ZnO sprayed thin films for optoelectronic applications. Opt. Mater. **154**, 115785 (2024). https://doi.org/10.1016/j.optmat.2024.115785
14. W. Darenfad, N. Guermat, K. Mirouh, Thoughtful investigation of ZnO doped Mg and co-doped Mg/Mn, Mg/Mn/F thin films: A first study. J. Mol. Struct. **1286**, 135574 (2023). https://doi.org/10.1016/j.molstruc.2023.135574
15. S. Jaballah, H. Dahman, I. Ghiloufi, G. Neri, L. El Mir, Facile synthesis of Al-Mg co-doped ZnO nanoparticles and their high hydrogen sensing performances. Int. J. Hydrog. Energy **45**, 34268–34280 (2020). https://doi.org/10.1016/j.ijhydene.2020.09.053
16. N. Guermat, W. Darenfad, K. Mirouh, M. Khalfallah, M. Ghoumazi, Super-hydrophobic F-doped SnO_2 (FTO) nanoflowers deposited by spray pyrolysis process for solar cell applications. J. Nano-Electron. Phys. https://doi.org/10.21272/jnep.14(5).05013
17. W. Darenfad, N. Guermat, K. Mirouh, A comparative study on the optoelectronic performance of undoped, Mg-doped and F/Mg co-doped ZnO nanocrystalline thin films for solar cell applications. J. Nano. Electron. Phys. (2021). https://doi.org/10.21272/jnep.13(6).06016
18. W. Darenfad, N. Guermat, N. Bouarissa, K. Mirouh, Investigation of structural, morphological and optoelectronic properties of (Ni, Co)-doped and (Ni/Co) co-doped SnO_2 (110) sprayed thin films. J. Mol. Struct. **1317**, 138992 (2024). https://doi.org/10.1016/j.molstruc.2024.138992
19. J. Zeng, H. Fan, J. Xue, Y. Wang, White-light luminescence properties of Mg and Sn doped ZnO prepared by thermal oxidation. Mater. Res. Bull. **50**, 421–423 (2014). https://doi.org/10.1016/j.materresbull.2013.11.007
20. F.H. Wang, M.S. Chen, Y.L. Jiang, H.W. Liu, T.K. Kang, Fabrication and characterization of sputtered Mg and F co-doped ZnO thin films with different substrate temperature for silicon thin-film solar cell applications. J. Alloy. Compd. **897**, 163174 (2022). https://doi.org/10.1016/j.jallcom.2021.163174
21. A. Tiwari, P.P. Sahay, The effects of Sn–In co-doping on the structural, optical, photoluminescence and electrical characteristics of the sol-gel processed ZnO thin films. Opt. Mater. **110**, 110395 (2020). https://doi.org/10.1016/j.optmat.2020.110395
22. A. El Hamidi, E. El Mahboub, K. Meziane, A. El Hichou, A. Almaggoussi, The effect of electronegativity on optical properties of Mg doped ZnO. Optik **241**, 167070 (2021). https://doi.org/10.1016/j.ijleo.2021.167070

23. E. Aslan, M. Zarbali, Tuning of photosensitivity and optical parameters of ZnO based photodetectors by co-Sn and Ti doping. Opt. Mater. **125**, 112030 (2022). https://doi.org/10.1016/j.optmat.2022.112030
24. W. Darenfad, N. Guermat, N. Bouarissa, F.Z. Satour, A. Zegadi, K. Mirouh, Improvement in optoelectronics and photovoltaic properties of p-Co_3O_4/n-ZnO hetero-junction: effect of deposition time of sprayed Co_3O_4 thin films. J. Mater. Sci. Mater. Electron. **35**(162), 1–13 (2024). https://doi.org/10.1007/s10854-023-11909-2
25. Y. Nezzari, W. Darenfad, K. Mirouh, N. Guermat, N. Bouarissa, R. Merah, Hydrophobic nickel doped Co_3O_4 sprayed thin films as solar absorber. Opt. Quant. Electron. **56**, 951 (2024). https://doi.org/10.1007/s11082-024-06930-6
26. I. Benaicha, I. Jellal, J. Mhalla, A. Fahmi, M. Addou, A. Qachaou, M. Fahoume, Atmospheric growth of ZnO thin films doped and co-doped with Ni and Co via UMVD: experimental and theoretical study. J. Mater. Sci. Mater. Electron. **33**, 6999–7010 (2022). https://doi.org/10.1007/s10854-022-07880-z
27. A. Bedia, F.Z. Bedia, M. Aillerie, N. Maloufi, Structural, electrical and optical properties of Al–Sn codoped ZnO transparent conducting layer deposited by spray pyrolysis technique. Superlattices Microstruct. **111**, 714–721 (2017). https://doi.org/10.1016/j.spmi.2017.07.031
28. D.D. Thongam, J. Gupta, N.K. Sahu, Effect of induced defects on the properties of ZnO nanocrystals: surfactant role and spectroscopic analysis. SN Appl. Sci. **1**, 1030 (2019). https://doi.org/10.1007/s42452-019-1058-3
29. R. Vettumperumal, S. Kalyanaraman, B. Santoshkumar, R. Thangavel, Estimation of electron–phonon coupling and Urbach energy in group-I elements doped ZnO nanoparticles and thin films by sol–gel method. Mater. Res. Bull. **77**, 101–110 (2016). https://doi.org/10.1016/j.materresbull.2016.01.015
30. R. Jothilakshmi, V. Ramakrishnan, R. Thangavel, J. Kumar, A. Sarua, M. Kuball, Micro-Raman scattering spectroscopy study of Li-doped and undoped ZnO needle crystals. J. Raman Spectros. **40**(5), 556–561 (2009). https://doi.org/10.1002/jrs.2164
31. A. Tiwari, P.P. Sahay, Improved transparent conductive properties of highly c-axis oriented ZnO thin films upon (Ga, Mg) co-doping. Micro Nanostruct. **181**, 207617 (2023). https://doi.org/10.1016/j.micrna.2023.207617
32. W. Nowicki, The interfacial energy in the Cassie-Baxter regime on the pyramid decorated solid surface. Eur. Phys. J. E **42**, 84 (2019). https://doi.org/10.1140/epje/i2019-11848-1
33. W. Darenfad, N. Guermat, K. Mirouh, Deposition time dependent physical properties of semiconductor CuO sprayed thin films as solar absorber. Eur. Phys. J. Appl. Phys. **99**, 17 (2024). https://doi.org/10.1051/epjap/2024230200
34. B. Sharma, R. Gupta, A. Chowdhuri, M. Tomar, Investigating mechanism of photo refractivity in Mg substituted ZnO thin films using pump and probe technique. Mat. Chem. Phys. **319**, 129375 (2024). https://doi.org/10.1016/j.matchemphys.2024.129375
35. O. Karzazi, L. Soussi, A. Louardi, A. El Bachiri, M. Khaidar, M. Monkade, H. Erguig, M. Taleb, Transparent conducting properties of Mg and Al co-doped ZnO thin films deposited by spray pyrolysis technique. Superlattices Microstruct. **127**, 61–65 (2019). https://doi.org/10.1016/j.spmi.2018.03.011
36. K. Huang, Z. Tang, L. Zhang, J. Yu, J. Lv, X. Liu, F. Liu, Preparation and characterization of Mg-doped ZnO thin films by sol–gel method. Appl. Surf. Sci. **258**, 3710–3713 (2012). https://doi.org/10.1016/j.apsusc.2011.12.011
37. M.I. Lee, M.C. Huang, D. Legrand, G. Lerondel, J.C. Lin, Structure and characterization of Sn, Al co-doped zinc oxide thin films prepared by sol-gel dip-coating process. Thin Solid Films **570**, 516–526 (2014). https://doi.org/10.1016/j.tsf.2014.04.051
38. A. Tiwari, P.P. Sahay, Sn-Ga co-doping in sol-gel derived ZnO thin films: studies of their microstructural, optical, luminescence and electrical properties. Mater. Sci. Semicond. Process. **118**, 105178 (2020). https://doi.org/10.1016/j.mssp.2020.105178
39. A. Tiwari, P.P. Sahay, Modification in the physical properties of nanocrystalline ZnO thin films by Sn/Ni co-doping for transparent conductive oxide applications. Physica B **629**, 413638 (2022). https://doi.org/10.1016/j.physb.2021.413638
40. Z.Q. Ma, W.G. Zhao, Y. Wang, Electrical properties of Na/Mg co-doped ZnO thin films. Thin Solid Films **515**, 8611–8614 (2007). https://doi.org/10.1016/j.tsf.2007.03.119
41. H. Zhang, W. Li, G. Qin, H. Ruan, Z. Huang, F. Wu, C. Kong, L. Fang, Role of zinc interstitial defects in indium and magnesium codoped ZnO transparent conducting films. Appl. Surf. Sci. **492**, 392–398 (2019). https://doi.org/10.1016/j.apsusc.2019.06.245
42. S. Yılmaz, İ Polat, Y. Atasoy, E. Bacaksız, Structural, morphological, optical and electrical evolution of spray deposited ZnO rods co-doped with indium and sulphur atoms. J. Mater. Sci. Mater. Electron. **25**, 1810–1816 (2014). https://doi.org/10.1007/s10854-014-1803-8
43. S.W. Shin, I.Y. Kim, G.V. Kishor, Y.Y. Yoo, Y.B. Kim, J.Y. Heo, G.S. Heo, P.S. Patil, J.H. Kim, J.Y. Lee, Development of flexible Mg and Ga co-doped ZnO thin films with wide

band gap energy and transparent conductive characteristics. J. Alloy. Compd. **585**, 608–613 (2014). https://doi.org/10.1016/j.jallcom.2013.09.133

44. A. Tiwari, P.P. Sahay, Highly c-axis oriented (Mg, Sn) co-doped ZnO thin films for optoelectronic applications. Opt. Mater. **134**, 13098 (2022). https://doi.org/10.1016/j.optmat.2022.113098
45. F.J. Serrao, N.N. Bappalige, K.M. Sandeep, S. Raghavendra, Dominance of c-axis orientation on the carrier transport properties of Sn doped ZnO thin films. Thin Solid Films **722**, 138579 (2021). https://doi.org/10.1016/j.tsf.2021.138579
46. M.R. Rahman, M.N.H. Mia, M.N. Uddin, T. Ashrafy, M. Hoq, F. Alam, A.H. Jala, Conductive and optically transparent sol–gel spin coated Al^{3+} and Sn^{4+} doped ZnO nanocrystalline thin-films. J. Mater. Sci. Mater. Electron. **35**, 1618 (2024). https://doi.org/10.1007/s10854-024-13328-3
47. Y. Zhu, Y. Wu, F. Cao, X. Ji, Ga-concentration-dependent optical and electrical properties of Ga-doped ZnO thin films prepared by low-temperature atomic layer deposition. J. Mater. Sci. Mater. Electron. **33**, 5696–5706 (2022). https://doi.org/10.1007/s10854-022-07756-2

Publisher's Note Springer Nature remains neutral with regard to jurisdictional claims in published maps and institutional affiliations.

Springer Nature or its licensor (e.g. a society or other partner) holds exclusive rights to this article under a publishing agreement with the author(s) or other rightsholder(s); author self-archiving of the accepted manuscript version of this article is solely governed by the terms of such publishing agreement and applicable law.